ISSN (Print) 1226-1750
ISSN (Online) 2233-6656
Journal of Magnetics 30(4), 694-701 (2025) https://doi.org/10.4283/JMAG.2025.30.4.694

Effect of BMI-related Noise on Liver Fat Quantification and Coronary Artery Calcium Scoring in Electromagnetic X-ray Computed Tomography Images

Hajin Kim[1], Sewon Lim[1], Minji Park[1], Jina Shim[2], Caterina Battaglia[3], Kyuseok Kim[4]*, and Youngjin Lee[5]*

[1]Department of Health Science, General Graduate School of Gachon University, 191, Hambakmoero, Yeonsu-gu, Incheon 21936, Republic of Korea
[2]Department of Radiotechnology, Wonkwang Health Science University, 514, Iksan-daero, Iksan-si, Jeonbuk-do 54538, Republic of Korea
[3]Department of Experimental and Clinical Medicine, Magna Graecia University, Viale Europa, 88100 Catanzaro, Italy
[4]Institute of Human Convergence Health Science, Gachon University, 191, Hambakmoero, Yeonsu-gu, Incheon 21936, Republic of Korea
[5]Department of Radiological Science, Gachon University, 191, Hambakmoero, Yeonsu-gu, Incheon 21936, Republic of Korea

(Received 16 September 2025, Received in final form 8 December 2025, Accepted 9 December 2025)

This study investigated the effects of body mass index (BMI)-related noise simulation on coronary artery calcium score (CACS) and liver fat quantification in coronary artery computed tomography (CT) images, which are acquired using X-ray-based electromagnetic radiation. Noise maps extracted from obese patients were added to normal-weight images to generate virtual high-BMI conditions, allowing assessment of noise effects independent of anatomical differences. CACS was evaluated at four locations, and liver fat was quantified using liver attenuation, liver-to-spleen (L/S) ratio, and L/S difference. Across the virtual high-BMI datasets, approximately 71% of cases showed increased CACS and 57% demonstrated upward changes in risk rank. Liver fat assessment decreased by up to 1.98%, 6.69%, and 19.02% in liver attenuation, L/S ratio, and L/S difference, respectively. These findings indicate that BMI-related noise, arising from increased attenuation of electromagnetic X-ray photons, can influence quantitative CT metrics and should be considered in clinical CT interpretation.

Keywords : electromagnetic radiation, x-ray attenuation, BMI-related noise, calcium scoring, liver attenuation

1. Introduction

Cardiovascular disease is one of the leading causes of death worldwide, accounting for approximately 19.41 million deaths in 2021. Among these, coronary artery disease (CAD) accounts for the largest proportion, with approximately 370,000 deaths in the United States by 2022 caused by CAD [1].

Coronary artery calcification (CAC) is considered a major imaging marker reflecting CAD progression, and coronary artery computed tomography (CT) is used to quantify the coronary artery calcium score (CACS) using the Agatston score to assess cardiovascular risk [2-4]. The CACS, based on the predominantly used Agatston score, is generally measured as high attenuation areas exceeding 130 Hounsfield units (HU) on CT images as calcified lesions; it calculates the score by multiplying the lesion area and the density factor based on the maximum HU value, classifies the patient's risk level, and sets up an appropriate treatment plan. This method reflects both the size and density of calcified lesions and is widely used in clinical settings as a standard quantification tool [5-7].

Coronary artery CT for CACS measurement is generally conducted under standardized conditions. CT imaging generates X-ray photons through the acceleration of electrons toward a metal target in an X-ray tube, a process fundamentally governed by electromagnetic X-ray. However, in obese patients, increased body fat tissue results in increased X-ray scattering and attenuation, leading to increased image noise. This noise can appear

*Corresponding author: Tel: +82-32-820-4360,
Fax: +82-32-820-4449, e-mail: kskim502@gachon.ac.kr (K. Kim)
Tel: +82-32-820-4362, Fax: +82-32-820-4449,
e-mail: yj20@gachon.ac.kr (Y. Lee)

as a high-density signal exceeding HU 130 in the image and may be recognized as similar to actual calcified lesions, resulting in an overestimated Agatston score [8].

Recent preliminary studies highlighted the relationship between CAD (particularly CAC) and fatty liver. As a representative disease, non-alcoholic fatty liver disease (NAFLD) is closely associated with various cardiovascular risk factors, including metabolic syndrome, insulin resistance, hypertension, and dyslipidemia. In addition, numerous cohort studies demonstrated that fatty liver disease, including NAFLD, is also associated with an increased incidence of CAC and CAD [9-11].

In clinical practice, for a quantitative assessment of liver fat based on CT images, the absolute liver attenuation value, liver-to-spleen ratio (L/S ratio), and liver-to-spleen difference (L/S difference) are generally measured on abdominal CT images without contrast enhancement [12-14]. According to the results of one study, the attenuation value of the overall liver can be represented in the upper part of the liver, as shown in coronary artery CT images [15]. Because CT attenuation arises from electromagnetic interactions between X-ray photons and tissue electrons, variations in liver fat content can directly alter the measured HU values. However, no studies have quantitatively evaluated the liver attenuation using coronary artery CT images, and few studies have analyzed the relationship between the CACS and liver fat assessment methods. In addition, although numerous studies have previously compared CACS differences between normal-weight and obese patients, simultaneous evaluation of liver fat and CACS using coronary artery CT has not been conducted [16-18].

Therefore, in this preliminary study, we applied three liver fat quantification methods to normal-weight patient images and their corresponding virtual high-body mass index (BMI) conditions generated using BMI-related noise simulation. This approach enabled us to compare and evaluate the tendencies of CACS and liver fat assessment methods in response to BMI-related noise while excluding anatomical differences.

2. Materials and Methods

2.1. Computed tomography image acquisition

This retrospective study was approved by the Institutional Review Board of Severance Hospital (4-2023-1221), which waived the need for informed consent owing to its retrospective design.

Coronary artery CT images were acquired from seven normal-weight patients using a Somatom Definition Force scanner (Siemens Healthineers, Erlangen, Germany). The primary scan parameters were as follows: tube voltage of 100 kVp, tube current of 80 mAs, scan time of 0.14 s, rotation time of 0.25 s, slice thickness/increment of 3.0/1.5 mm, field of view of 300 mm. The reconstruction kernel was Qr36f, and a reconstruction window set to mediastinum. The images were reconstructed in an 512 × 512 matrix using sequence scan mode in the craniocaudal direction.

According to the World Health Organization (WHO) guidelines, the classification of patient groups is as follows: normal-weight is defined as a BMI of ≤ 25 kg/m^2, and obesity is defined as a BMI of ≥ 30 kg/m^2 [19]. Therefore, in this study, we followed the WHO guidelines and selected 15 patients with a BMI of 27-39 kg/m^2 as the obese group.

In addition, to analyze the effects of image noise caused by an increase in BMI and exclude the influence of tissue structure or anatomical differences in the images, noise maps extracted from the images of 15 obese patients were added to the coronary artery CT images of normal-weight patients to generate virtual high-BMI conditions.

2.2. Modeling of Poisson-Gaussian mixture noise estimation algorithm

To extract noise from CT images of obese patients, we modeled and applied a Poisson–Gaussian mixed noise algorithm [20, 21]. To extract noise, the CT images of the obese patients were divided into uniform patches, and the mean and standard deviation of each patch were estimated. The global functional relationship between the image intensity and noise standard deviation was determined using a regression analysis of the estimated values for each patch. The equations for the Poisson-Gaussian mixture model are given in Eqs. (1) and (2):

$$A(x) = z(x) + n(z(x))\sigma \tag{1}$$

$$n^2(z(x)) = \alpha z(x) + \beta^2 \tag{2}$$

where x represents the pixel location, $z(x)$ represents the noise-free signal value at that location, and $A(x)$ represents the observed degraded signal at the same location. Furthermore, $n(z(x))$ denotes the standard deviation of the noise distribution, and σ is the independent random noise with a mean of 0 and a standard deviation of 1. Additionally, α represents the signal-dependent Poisson noise and β represents the standard deviation of the signal-independent Gaussian noise.

To estimate the values of α and β, we employed a patch-based noise parameter estimation method that demonstrated high accuracy in previous studies. For noise level estimation, homogeneous patches of the image were identified using a nonparametric statistical method,

specifically Kendall's tau rank correlation, which quantifies the consistency of pixel intensity relationships within a patch [22]. Patches with high homogeneity, in which variations were assumed to arise primarily from noise, were selected on the basis of this measure. The Kendall's tau was computed using Eq. (3):

$$T = C - D/C + D' \tag{3}$$

where C and D are the number of concordant and discordant pairs, and T is in the range of -1 to 1. The homogeneous patches were 16 × 16 pixels in size and were detected by averaging the four directional T values. Each selected homogeneous patch was characterized by its mean (μ) and standard deviation (δ). These statistical values were used to model a noise estimation model, as described in Equations (4–6), and finally, optimal values of the noise parameters α and β^2 were estimated:

$$f^* = arg \min_{f \in R^+} \|Uf - V\|_1 \tag{4}$$

$$f = \begin{pmatrix} \alpha \\ \beta^2 \end{pmatrix} \tag{5}$$

$$U = \begin{pmatrix} \mu_1 & 1 \\ \mu_2 & 1 \\ \vdots & \vdots \\ \mu_N & 1 \end{pmatrix}, V = \begin{pmatrix} \delta_1^2 \\ \delta_2^2 \\ \vdots \\ \delta_N^2 \end{pmatrix} \tag{6}$$

where, f represents the noise level parameter vector that satisfies the feasible sets $f \in R^+$, and U and V are mean of $N \times 2$ and variance of $N \times 1$ matrix, respectively.

The minimization problem was solved using a pre-conditioned primal-dual algorithm, which enabled the estimation of Poisson noise α and Gaussian noise β^2. The values of α and β^2 extracted from obese patients are shown in Table 1, and the overall flowchart is shown in Fig. 1.

Table 1. Estimated Poisson (α) and Gaussian (β^2) noise parameters extracted from computed tomography images of obese patients.

Obese	Poisson parameter (α)	Gaussian parameter (β^2)
Patient 1	0.17	10.59
Patient 2	0.21	11.62
Patient 3	0.17	10.22
Patient 4	0.15	9.74
Patient 5	0.16	11.31
Patient 6	0.38	12.57
Patient 7	0.33	12.42
Patient 8	0.39	12.60
Patient 9	0.36	14.04
Patient 10	0.23	11.10
Patient 11	0.27	10.67
Patient 12	0.33	12.27
Patient 13	0.27	10.42
Patient 14	0.19	10.29
Patient 15	0.25	11.36
Average ± SD	0.26 ± 0.08	11.41 ± 1.17
Median	0.25	11.31
Minimum, Maximum	[0.15, 0.39]	[9.74, 14.04]
95% Confidence interval	[0.21, 0.30]	[10.77, 12.06]

2.3. Calculation of coronary artery calcium scoring

To evaluate the effect of BMI-related noise on the CACS, noise extracted from actual obese patients was added to the coronary CT images of normal-weight patients to obtain virtual high-BMI conditions. A radiologist with 14 years of experience independently performed CACS on both the normal-weight and virtual high-BMI conditions. The calcium score was measured using syngo.via (version VB40; Siemens Healthcare, Erlangen, Germany), which automatically highlights and identifies areas with HU values exceeding 130, and calculates the Agatston score based on the mass and volume information of those areas.

The CACS analysis was performed at four locations: the left main trunk, left anterior descending artery, circumflex artery, and right coronary artery.

2.4. Assessment of liver fat content

To quantitatively evaluate changes in liver fat content under BMI-related noise simulation, three CT-based liver fat assessment methods were measured and compared between normal-weight and virtual high-BMI conditions: liver attenuation, L/S ratio, and L/S difference [12, 14, 23]. Liver attenuation refers to the average HU value measured within the liver, with lower HU values indicating higher fat accumulation. The L/S ratio was calculated by dividing the mean liver HU value by the mean spleen HU value, which reflected the relative attenuation between the two organs. The L/S difference was defined as the difference between the mean liver HU and mean spleen HU, representing the absolute attenuation difference.

To obtain consistent measurements, ten CT slices containing both the liver and spleen were selected for each patient. In each image, four circular regions of interest (ROIs) with fixed radii of 20 pixels were placed in the liver, and one ROI was placed in the spleen. During ROI definition, particular care was taken to include only

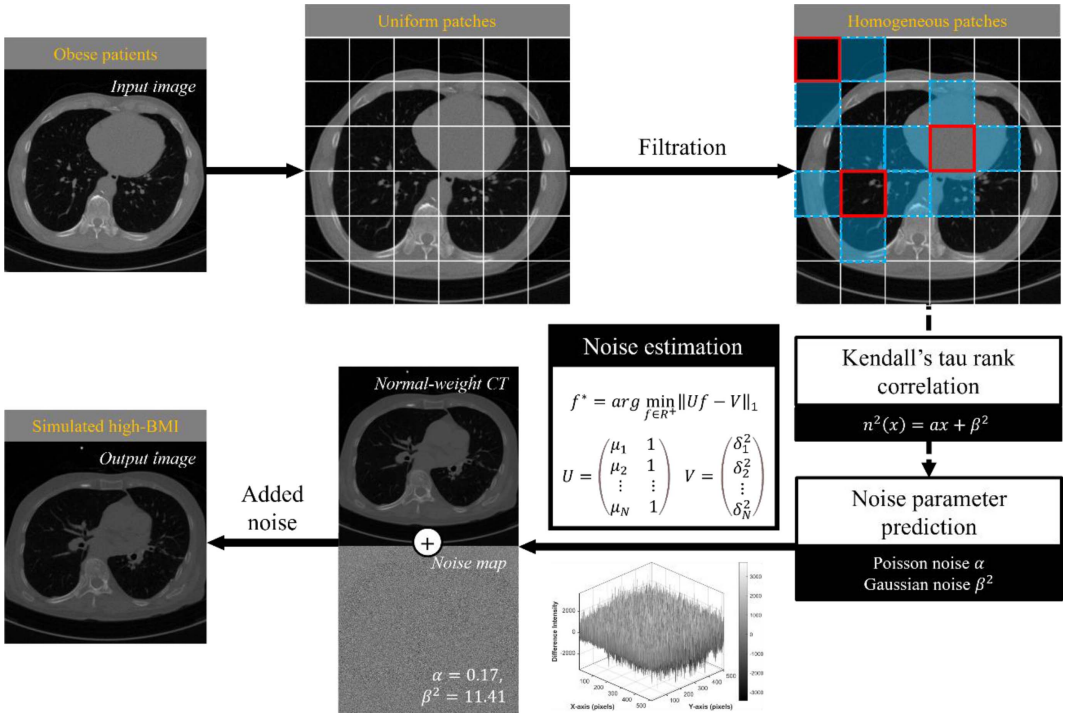

Fig. 1. (Color online) Overview flowchart of the noise estimation and data acquisition process of virtual high-BMI conditions.

hepatic parenchyma. Consequently, vascular structures, calcifications, perihepatic fat tissue, and biliary ductal structures were systematically excluded. Furthermore, any detectable focal lesions or masses were carefully omitted to ensure that only representative liver tissue was incorporated into the quantitative analysis. To verify the appropriateness and consistency of these ROI placements, all selected regions were additionally reviewed and confirmed by a radiologist. The average values of these ROIs were used to calculate the three evaluation methods. Fig. 2 shows the locations of ROIs in the liver and spleen.

3. Results and Discussion

When comparing the CACS values between normal-weight and virtual high-BMI conditions, five patients exhibited higher CACS values in the simulated high-BMI condition. The CACS values of normal-weight patients

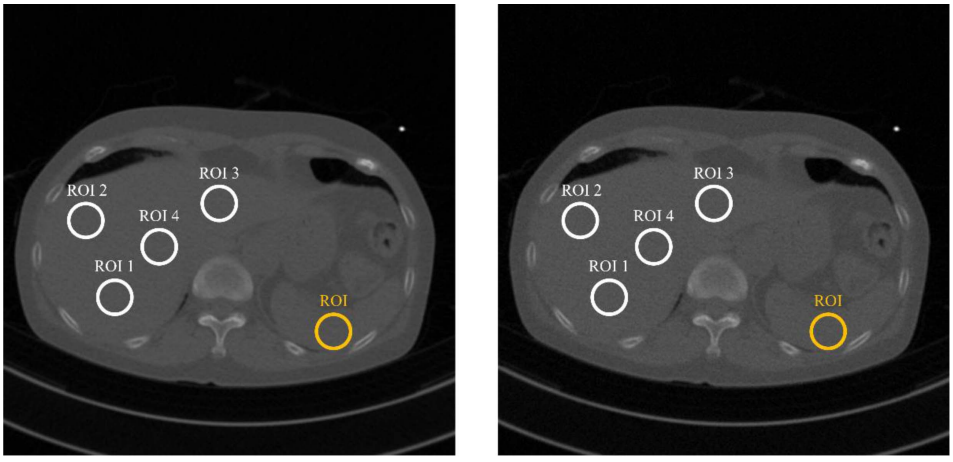

(a) (b)

Fig. 2. (Color online) Region of interest (ROI) setting for measuring liver fat content: (a) normal-weight patient, and (b) virtual high-BMI conditions. The four white circles represent the ROI of the liver, and the yellow circle represents the ROI of the spleen.

Table 2. Coronary artery calcium score (CACS) and risk rank evaluation values for normal-weight and virtual high-BMI conditions. Risk rank categories were classified based on CACS as follows: rank 1: CACS = 0; rank 2: 0 < CACS ≤ 10; rank 3: 10 < CACS ≤ 100; rank 4: 100 < CACS ≤ 400; rank 5: 400 < CACS

Patients	Weight	CACS	Risk rank
Patient 1	Normal	0.00	1
	High-BMI	0.00	1
Patient 2	Normal	0.50	2
	High-BMI	0.50	2
Patient 3	Normal	0.00	1
	High-BMI	0.83	2
Patient 4	Normal	5.90	2
	High-BMI	10.90	3
Patient 5	Normal	8.40	2
	High-BMI	11.56	3
Patient 6	Normal	9.80	2
	High-BMI	13.80	3
Patient 7	Normal	25.10	3
	High-BMI	32.40	3

ranged from 0.00 to 25.10; however, those of virtual high-BMI conditions showed values up to 32.40. In particular, in the case of patient 3, the CACS increased from 0.00 to 0.83, changing the risk rank from 1 to 2. In the case of patient 4, the CACS also increased from 5.90 to 10.90, in patient 5, the CACS increased from 8.40 to 11.56, and in patient 6, the CACS increased from 9.80 to 13.80, changing the risk rank from 2 to 3. We found that CACS tended to appear higher when BMI-related noise was generated in the CT images. The changes in the CACS of normal-weight patients and virtual high-BMI conditions are shown in Table 2 and Fig. 3.

To evaluate the relationship between BMI-related noise and liver fat content based on CT images, three liver fat content quantification methods—liver HU, L/S ratio, and L/S difference—were evaluated in both normal-weight and virtual high-BMI conditions (Fig. 4). In most patients, decreases in all three methods were observed under the virtual high-BMI condition, which may indicate a potential influence of the added noise in liver fat assessment.

The liver HU measurement indicated that six virtual high-BMI conditions exhibited lower HU values compared with the normal-weight patients. Patient 1, the only case with a slightly higher HU value, showed a small rise from 65.64 to 65.79. In all patients except Patient 1, the attenuation value of liver HU was reduced by an average of 0.94%, and in Patient 2, the HU value was reduced by

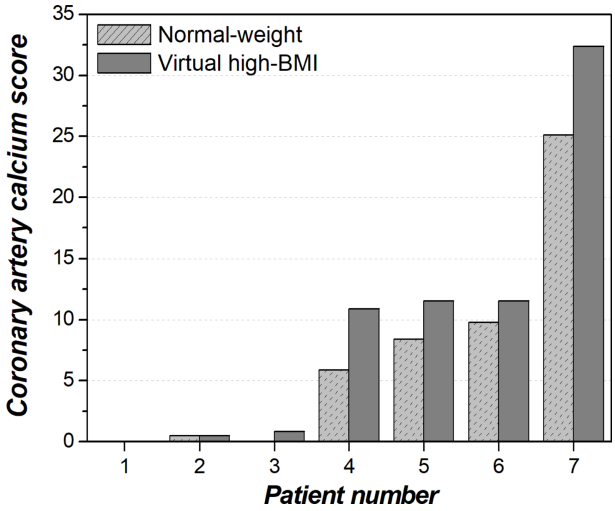

Fig. 3. Results of coronary artery calcium score measurements in normal-weight and virtual high-BMI conditions.

a maximum of 1.98% from 70.08 to 68.70.

The L/S ratio values were observed to be lower in all patients, with an average reduction of 1.74%. In particular, Patient 3 showed a tendency to decrease from 1.37 to 1.28, with a maximum observed reduction of approximately 6.69%.

The L/S difference values were measured to be lower in all patients, with an average reduction of 6.08%. Specifically, in Patient 3, the L/S difference showed a notable tendency to decrease from 17.28 to 13.99, and a maximum reduction observed across all patients was approximately 19.02%.

This study analyzed the effects of BMI-related noise on CACS and liver fat quantification in coronary artery CT images. By adding noise parameters derived from obese patients to the images of normal-weight patients, we aimed to assess the influence of noise alone, independent of anatomical differences. A tendency toward higher CACS values was noted in most virtual high-BMI conditions, and several patients exhibited changes in risk score, suggesting that BMI-related noise may have an impact on clinical evaluation. In addition, liver attenuation, L/S ratio, and L/S difference, which are commonly used methods for CT-based quantification of liver fat content, were generally measured to be lower under the virtual high-BMI condition, which may reflect the influence of increased BMI-related noise on liver fat assessment. Among these methods, the L/S difference tended to show the largest relative reduction, suggesting that it may be more sensitive to BMI-related noise compared with the other indices (Fig. 5).

Our studies showed that BMI-related noise in CT

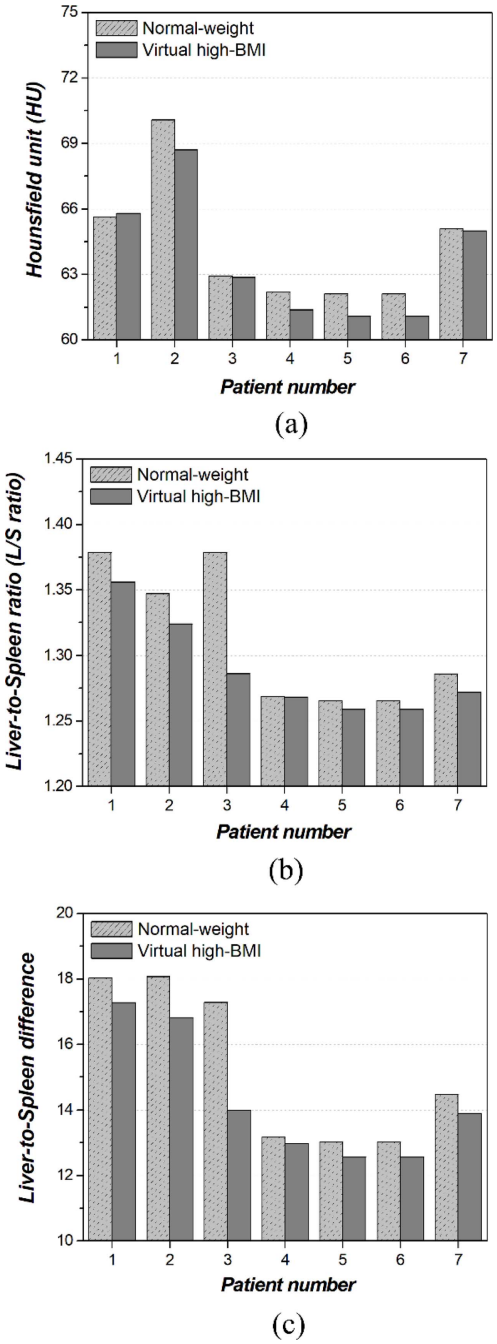

Fig. 4. Results of liver fat quantification methods between normal-weight and virtual high-BMI conditions: (a) liver attenuation values (HU), (b) liver-to-spleen ratio (L/S ratio), and (c) liver-to-spleen difference (L/S difference).

images generates artificial high-intensity signals similar to CAC, which can overestimate CACS values. Therefore, advanced algorithms that separate noise artifacts from CAC are required. Several previous studies have proposed deep learning-based noise reduction methods that learn the statistical distribution of noise using data-driven

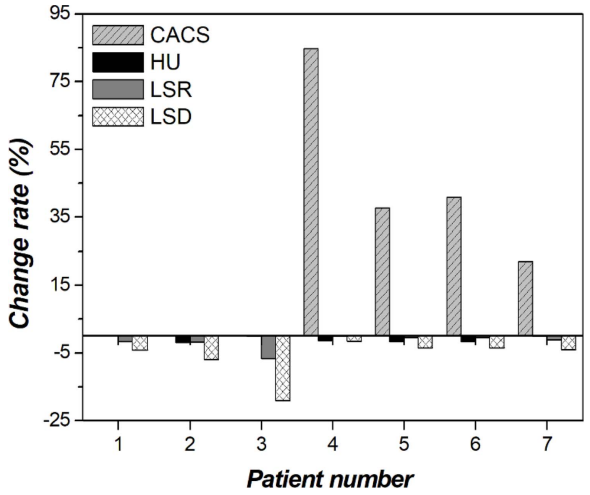

Fig. 5. Change rates (%) of coronary artery calcium score (CACS), liver attenuation (HU), liver-to-spleen ratio (LSR), and liver-to-spleen difference (LSD) between normal-weight and virtual high-BMI conditions.

training. The noise-to-noise training method enables the model to learn noise characteristics without reference images, showing promising results for noise reduction in low-dose CT images [24, 25]. In addition, generative adversarial networks have been used to model and suppress noise by learning the complex distribution of signals and noise through adversarial training and preserving essential anatomical details [26, 27]. These approaches highlight the potential of deep learning models trained on noise statistics and characteristics. Given that CT noise originates from the quantum behavior of X-ray photons—a form of electromagnetic radiation—deep learning models that explicitly learn photon-statistics–based noise distributions may be particularly effective for mitigating BMI-related noise effects. Therefore, future studies could investigate whether applying such methods to coronary artery CT using datasets that include both calcified lesions and synthetic noise patterns can reduce noise-induced biases in CACS under high-BMI conditions.

Previous studies evaluated liver fat content on abdominal CT images and investigated the association between liver steatosis and CAD [28, 29]. Nevertheless, this is the first study, to our knowledge, to quantitatively analyze the association between CACS and liver fat content using coronary artery CT images. Moreover, this study is the first preliminary investigation to explore this association and provides a foundation for future clinical validation.

Studies on automatic liver fat analysis using deep learning have been actively conducted, but the selection of ROIs in clinical practice is almost always performed

manually. Many studies demonstrated that the selection of three ROIs rather than a single ROI is useful for quantitatively evaluating liver fat content in CT images [13, 30]. In this study, the liver ROI, which could cause variability, was manually selected. Therefore, in the future, we plan to investigate which ROI ranges and sizes affect liver fat content assessment. Moreover, we aimed to develop an automatic ROI-localization model using deep learning trained to identify the most stable ROI position.

As a preliminary study, this research observed the tendencies of CACS and liver fat content assessment methods under BMI-related noise simulation. However, it has the limitation of analyzing only seven patients, and the small sample size did not allow for statistical analysis. Therefore, in future study, we plan to include a larger cohort with more granular BMI stratification and to perform formal statistical analyses to enhance the validity and generalizability of our findings. Furthermore, an explicit limitation of our study is that anatomical and HU attenuation changes associated with true obesity were not modeled. Although our approach enabled noise-focused analysis, actual obese patients have anatomical variability that can affect measurements, such as fat distribution changes, organ displacement, and tissue heterogeneity [31]. Therefore, further validation using actual obese patient data is required, and future studies should categorize patients according to BMI class (e.g., normal, overweight, and obese) to investigate how anatomical and noise characteristics jointly affect the CACS and liver fat quantification. Accordingly, the present findings should be interpreted as preliminary noise-induced HU attenuation trends rather than as actual clinical effects of obesity.

This study was performed using CT data from a single scanner, which limits its generalizability to other scanners and clinical settings. Previous studies have shown that liver HU values differ among various scanners because of differences in reconstruction algorithms and tube currents [32, 33]. Since electromagnetic wave attenuation and photon flux vary depending on scanner design and acquisition parameters, BMI-related noise characteristics may also differ across systems. Accordingly, there is a need for methods that can reduce scanner-related variability, and phantom-based HU normalization approaches performed under coronary artery CT conditions may be required to improve the consistency of attenuation measurements across different systems.

In this study, we used a noise estimation algorithm to simulate BMI-related noise in coronary artery CT images and modeled a noise estimation algorithm that separated the noise components. Using this algorithm, we extracted BMI-related noise characteristics from the obese patient group and applied them to generate synthetic datasets. Given these approaches, there is a need for approaches that can reduce BMI-related noise while preserving essential anatomical structures. Future study may require exploring whether deep learning frameworks trained on datasets that include calcified lesions alongside simulated BMI-related noise patterns could help reduce noise-induced bias in quantitative coronary CT analysis under varying BMI conditions.

Currently, coronary artery CT scans for CACS measurements are usually performed using a standardized clinical protocol, regardless of the patient's body size, and BMI is not considered. Therefore, diagnostic errors and unnecessary treatment plans for patients are a possibility [34]. Our results support the need for an image-processing pipeline that accounts for BMI-related noise. In particular, approaches that incorporate BMI as an additional imaging factor, potentially including deep learning-based noise correction strategies, may be needed to enable more consistent interpretation under patient-specific image conditions. In addition, exploring whether quantitative liver fat assessment can be interpreted along with CACS may provide useful insights for future cardiovascular risk evaluation. Examining the relationship between liver fat content and CACS in larger populations could help clarify their potential complementary value in risk stratification.

Overall, this study highlights the effects of BMI-related noise on two clinically important imaging biomarkers. Our findings suggest that CT-based assessments should incorporate noise reduction and anatomical normalization strategies to ensure accurate and personalized assessments. This approach highlights the importance of incorporating BMI-related noise considerations into CT image interpretation and may serve as a useful basis for future methodological refinements in quantitative imaging.

4. Conclusion

This study demonstrated that noise caused by increased BMI-related noise can affect CACS and liver fat quantification in coronary artery CT images. The results showed that the CACS increased in coronary artery CT images under virtual high-BMI conditions, and that all liver fat quantification methods tended to decrease, with the most pronounced decrease observed in the L/S difference method. Our analyses suggest that CT image noise associated with high BMI may lead to overestimation of the CACS and misclassification of risks in clinical assessment. Given that CT acquisition uses X-ray electromagnetic radiation, increased BMI affects photon attenu-

ation and contributes to the observed noise-related biases. These findings highlight the need for noise reduction techniques or BMI-based corrections in quantitative CT image analysis.

Funding

This study was supported by the Gachon University research fund of 2025 (GCU-202503280001) and was supported by a grant from the National Foundation of Korea (NRF) funded by the Korean government (Grant No. RS-2024-00354252).

References

[1] American Heart Association, 2025. Heart Disease and Stroke Statistics -2025 Update. https://www.heart.org/en/about-us/heart-and-stroke-association-statistics (accessed April 2025).
[2] H. S. Bhatia, R. L. McClelland, J. Denenberg, M. J. Budoff, M. A. Allison, and M. H. Criqui, Circ. Cardiovasc. Imaging **16**, e014788 (2023).
[3] P. Kumar and M. Bhatia, J. Cardiovasc. Imaging **31**, 1 (2023).
[4] O. H. Obisesan, A. D. Osei, S. M. I. Uddin, O. Dzaye, and M. J. Blaha, Radiol. Cardiothorac. Imaging **3**, e200484 (2021).
[5] K. Nasir, A. C. Razavi, and O. Dzaye, Circ. Cardiovasc. Imaging **16**, e015150 (2023).
[6] K. Y. Hou, K. Tsujioka, and C. C. Yang, J. Appl. Clin. Med. Phys. **21**, 111 (2020).
[7] M. J. Blaha, M. B. Mortensen, S. Kianoush, R. Tota-Maharaj, and M. Cainzos-Achirica, JACC Cardiovasc. Imaging **10**, 923 (2017).
[8] J. Shim, K. Kim, and Y. Lee, Appl. Sci. **14**, 8906 (2024).
[9] D. Kim, S.-Y. Choi, E. H. Park, W. Lee, J. H. Kang, W. Kim, Y. J. Kim, J.-H. Yoon, S. H. Jeong, D. H. Lee, H.-S. Lee, J. Larson, T. M. Therneau, and W. R. Kim, Hepatology **56**, 605 (2012).
[10] U. Arslan and M. Yenerçağ, World J. Clin. Cases **8**, 4688 (2020).
[11] K. C. Sung, T. K. Yoo, M. Y. Lee, C. D. Byrne, M. H. Zheng, and G. Targher, Arterioscler. Thromb. Vasc. Biol. **43**, 482 (2023).
[12] J. Starekova, D. Hernando, P. J. Pickhardt, and S. B. Reeder, Radiology **301**, 250 (2021).
[13] I. Zeb, D. Li, K. Nasir, R. Katz, V. N. Larijani, and M. J. Budoff, Acad. Radiol. **19**, 811 (2012).
[14] Y. Kodama, C. S. Ng, T. T. Wu, G. D. Ayers, S. A. Curley, E. K. Abdalla, J. N. Vauthey, and C. Charnsangaveh, AJR Am. J. Roentgenol. **188**, 1307 (2007).
[15] A. Gupta, K. Bera, E. Kikano, J. D. Pierce, J. Gan, M. Rajdev, L. M. Ciancibello, A. Gupta, S. Rajagopalan, and R. C. Gilkeson, RadioGraphics **42**, 947 (2022).
[16] C. K. Kramer, D. von Muhlen, J. L. Gross, and E. Barrett-Connor, The Journal of Clinical Endocrinology & Metabolism **94**, 5039 (2009).
[17] N. Ohashi, H. Yamamoto, J. Horiguchi, T. Kitagawa, N. Hirai, K. Ito, and N. Kohno, Atherosclerosis **202**, 192 (2009).
[18] C. D. Lee, D. R. Jacobs Jr, P. J. Schreiner, C. Iribarren, and A. Hankinson, The American Journal of Clinical Nutrition **86**, 48 (2007).
[19] World Health Organization, 2025. Obesity and overweight. https://www.who.int/news-room/fact-sheets/detail/obesity-and-overweight (accessed 9 April 2025).
[20] Q. Ding, Y. Long, X. Zhang, and J. A. Fessler, arXiv preprint. arXiv:1801.09533 (2018).
[21] S. Lee, M. S. Lee, and M. G. Kang, Sensors (Basel) **18**, 1019 (2018).
[22] C. Sutour, C. A. Deledalle, and J. F. Aujol, SIAM Journal on Imaging Sciences **8**, 2622 (2015).
[23] G. M. Bydder, R. W. G. Chapman, D. Harry, L. Bassan, S. Sherlock, and L. Kreel, J. Comput. Tomogr. **5**, 33 (1981).
[24] Y. Zhu, Q. He, Y. Yao, and Y. Teng, Pattern Recognit. **161**, 111285 (2025).
[25] D. Wu, K. Kim, and Q. Li, Med. Phys. **48**, 7657 (2021).
[26] Z. Huang, J. Zhang, Y. Zhang, and H. Shan, IEEE Trans. Instrum. Meas. **71**, 1 (2021).
[27] Q. Yang, P. Yan, Y. Zhang, H. Yu, Y. Shi, X. Mou, M. K. Kalra, Y. Zhang, L. Sun, and G. Wang, IEEE Trans. Med. Imaging **37**, 1348 (2018).
[28] R. Shi, X. Li, K. Sun, F. Liu, B. Kang, Y. Wang, Y. Wang, B. Zhu, X. Zhao, Z. Liu, and X. Wang, BMC Cardiovasc. Disord. **24**, 267 (2024).
[29] N. M. Meyersohn, T. Mayrhofer, K. E. Corey, D. O. Bittner, P. V. Staziaki, B. Szilveszter, T. Hallett, M. T. Lu, S. B. Puchner, T. G. Simon, B. Foldyna, D. Voora, G. S. Ginsburg, P. S. Douglas, U. Hoffmann, and M. Ferencik, Clin. Gastroenterol. Hepatol. **19**, 1480 (2021).
[30] Y. Huo, J. G. Terry, J. Wang, S. Nair, T. A. Lasko, B. I. Freedman, J. J. Carr, and B. A. Landman, Med. Phys. **46**, 3508 (2019).
[31] P. M. Graffy and P. J. Pickhardt, Br. J. Radiol. **89**, 20151024 (2016).
[32] R. D. Boutin, A. M. Hernandez, L. Lenchik, J. A. Seibert, D. A. Gress, and J. M. Boone, AJR Am. J. Roentgenol. **216**, 447 (2021).
[33] E. P. S. Sande, A. C. T. Martinsen, E. O. Hole, and H. M. Olerud, Phys. Med. Biol. **55**, 5123 (2010).
[34] J. C. Jensen, Z. A. Dardari, M. J. Blaha, S. White, L. J. Shaw, J. Rumberger, A. Rozanski, D. S. Berman, M. J. Budoff, K. Nasir, and M. D. Miedema, Circ. Cardiovasc. Imaging **13**, e009495 (2020).